CORA Cork Open Research Archive
Cartlann Taighde Oscailte Chorcaí

Title	Anisotropy of weak light scattering in thin opal films
Author(s)	Romanov, Sergei G.
Publication date	2008-05-13
Original citation	Romanov, S. G. (2008) 'Anisotropy of weak light scattering in thin opal films', Journal of Applied Physics, 103(9), pp. 093117. doi: 10.1063/1.2917224
Type of publication	Article (peer-reviewed)
Link to publisher's version	http://aip.scitation.org/doi/abs/10.1063/1.2917224 http://dx.doi.org/10.1063/1.2917224 Access to the full text of the published version may require a subscription.
Rights	**© 2008 American Institute of Physics, This article may be downloaded for personal use only. Any other use requires prior permission of the author and AIP Publishing. The following article appeared in Romanov, S. G. (2008) 'Anisotropy of weak light scattering in thin opal films', Journal of Applied Physics, 103(9), pp. 093117 and may be found at http://aip.scitation.org/doi/abs/10.1063/1.2917224**
Item downloaded from	http://hdl.handle.net/10468/4224

UCC

University College Cork, Ireland
Coláiste na hOllscoile Corcaigh

Anisotropy of weak light scattering in thin opal films

Sergei G. Romanov

Anisotropy of weak light scattering in thin opal films

Sergei G. Romanov[a)]
Tyndall National Institute, University College Cork, Prospect Row, Cork, Ireland and Ioffe Physical Technical Institute, Polytekhnicheskaya 26, St. Petersburg 192021, Russia

The forward and backward light scattering that accompanied the almost ballistic light propagation in opal-based three-dimensional photonic crystal (PhC) has been experimentally studied. The light path memory and the high anisotropy of scattering have been associated with low-order scattering at large-scale crystal defects. The strong backscattered light intensity has been linked to the uncoupled light at a PhC surface. The exponent of power-law approximation of angle diagrams of the scattered light intensity has been suggested as a measure of the scattering anisotropy. The scattering anisotropy spectra have demonstrated that in a vicinity to the first photonic bandgap, the lower directionality of the forward scattering is complemented by the higher directionality of the backward scattering. © *2008 American Institute of Physics.* [DOI: 10.1063/1.2917224]

I. INTRODUCTION

The crystal quality of three-dimensional (3D) photonic crystals (PhCs) varies depending on the preparation method, but none of the modern technologies is good enough to provide large size PhCs with ballistic light propagation. Hence, a collimated light beam traversing a 3D PhC drops a large fraction of its intensity due to scattering at intrinsic lattice defects. In 3D PhCs of macroscopic dimensions, the propagation becomes completely chaotic. This justifies the success of the random light scattering formalism borrowed from, e.g., the physics of atmosphere for interpretation of diffuse light propagation in PhCs.[1]

In random inhomogeneous media the order of scattering N is introduced to indicate the effective number of scattering events experienced by a photon. The diffuse approximation correctly describes the component of scattered light, which undergoes multiple scattering events. To describe the light propagation, the mean free path l^* and the transport length $l_{tr} = l^*/(1-g)$ are introduced. l_{tr} is the length necessary for complete randomization of the photon trajectory, which begins with the wavevector of the incident plane wave. g is the parameter of scattering anisotropy or the average cosine of the scattering angle α.[2] In a general form

$$g = 2\pi \int_0^\pi \cos\alpha \, p(\cos\alpha)\sin\alpha \, d\alpha, \tag{1}$$

where $p(\cos\alpha)$ is the phase function, which characterizes the scattering diagram of the light wave at a single particle. The Henyey–Greenstein phase function is often used to characterize the angular distribution of scattered light in random inhomogeneous medium:[3]

$$p(\cos\alpha) = \frac{1-g^2}{4\pi(1+g^2-2g\cos\alpha)^{3/2}}. \tag{2}$$

The meaning of $p(\cos\alpha)$ is that the probability of scattering within the angle interval $[\alpha, \alpha+d\alpha]$ is equal to

$$P_\alpha = 2\pi p(\cos\alpha)\sin\alpha \, d\alpha. \tag{3}$$

Isotropic scatterer is characterized by $g=0$ and the strongly anisotropied scattering occurs if $g \approx 1$. For a point scatterer ($d \ll \lambda$), $l^* = l_{tr}$, i.e., random direction of propagation can be found after the first collision. If $d \sim \lambda$, then $0 < g < 1$ and $l_{tr} > l^*$, i.e., correlation of the scattered flux with the direction of the incidence becomes lost after several collisions.[4] The diffuse flow of radiation forms if the medium size $t \gg l_{tr}$. As Monte Carlo simulations show, if $N=1,2$, the scattering intensity decreases by six orders of magnitude at the scattering angle $\alpha \geq 25°$,[5] where α is the angle between wavevectors of incident and scattered waves. Increase in the scattering order to $N \approx 10$ leads to 10^3 increase in the scattered light intensity. Backscattering at $N=1,2$ is negligibly low. It approaches level of $10^{-4}-10^{-5}$ of incident light intensity at $N=10-20$.

In the hypothetic case of a PhC with a perfectly ordered lattice, the light is ballistically transported by the lattice eigenmodes. In real-life lattices, the lattice defects add their own localized defect modes to the ensemble of crystal eigenmodes. If the density of defects is high enough for defect states to overlap, they also transport the light flow through the PhC. However, since the symmetry of defect modes differs from that of lattice eigenmodes, the light transported by them obeys different rules. In experiment, the change of the diffuse propagation to the ballistic one can be achieved along the decrease in the thickness of a PhC slab. However, this thickness cannot be reduced below a certain threshold, which is critical to the formation of a photonic bandgap (PBG) structure. Thin films of 3D PhCs prepared, e.g., by holography, two-photon polymerization, or self-assembling, represent the closest approximation to structures with ballistic light propagation. The thickness of such PhC films t is thin enough to fulfill the condition $t \leq l_{tr}$.

In this paper, the light scattering was studied in thin-film opal-based PhC,[6] which nowadays are very popular among researches. The light propagation in such films is far from being random, but it is not a purely ballistic one either. Moreover, the characteristics of the scattered light begin to

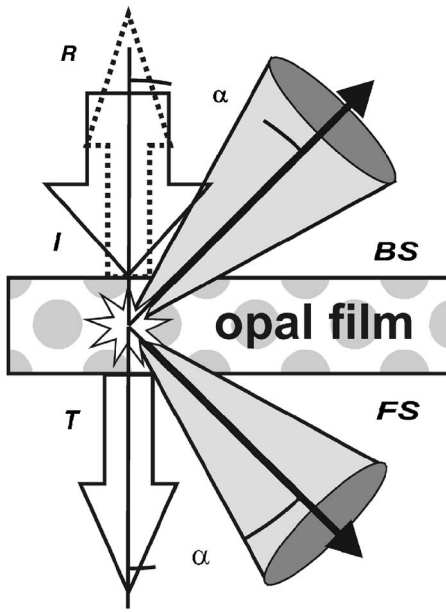[a)]Electronic mail: sergei.romanov@tyndall.ie.

FIG. 1. Schematics showing decomposition of the incident light on different components in the opal-based PhC with intrinsic defects.

depend on the dominating type of defects. So far, no theoretical calculations of the scattered light spectra in 3D PhCs were presented and reliable predictions are limited to disordered two-dimensional PhCs.[7] Therefore, experimental studies of light scattering in this mixed propagation regime are of general significance for the whole class of such 3D PhCs.

In opals the scattered light intensity (S) can be measured either directly[8,9] or calculated from a balance of the incident (I), transmitted (T), and reflected (R) light intensities.[10] The latter approach[8,10] neglects the complex character of losses, which consist of the backwardscattered (BS) and forward scattered (FS) light and the light trapped in the opal slab (TR) (Fig. 1):

$$I = T + R + S, \quad S = \text{BS} + \text{FS} + \text{TR}. \quad (4)$$

Opals can be characterized by a mixture of large size defects, such as grain and twin boundaries, and small size defects, such as deviations of sphere size from a mean diameter. Direct measurements of the scattered light intensity behind thick and thin opal slabs with moderate *RI* contrast have been reported elsewhere,[9,11] whereas backward scattering remains to be studied. In bulk opals with $t \gg l_{tr}$, where complete transformation of the directional beam into a diffuse light takes place, the light propagation is influenced by both the multiple scattering at lattice defects and the PBG, although the latter affects only the exit part of the photon trajectory.[9] The FS indicatrix or the angle diagram of the scattered light intensity is the Lambert-type diagram for all wavelengths, but along the PBG direction the scattered light intensity experiences attenuation. Depending on the RI contrast, the scattered light propagation appears suppressed in larger or smaller fraction of the hemisphere behind the thick opal slab. Typical features of FS light in thin-film opals are the superposition of several diffraction resonances along the incident and the scattered beam directions in scattering spectra and the narrow scattering indicatrix.[12] Infiltration of opal

with a *RI*-matching liquid brings opal back to a transparent state with the anisotropic scattering at grain boundaries, i.e., to the $d \gg \lambda$ regime, and narrow PBG projection cones.[13]

The aims of this paper are to compare the forward and backward scattered light in thin opal films and to estimate PBG influence upon the scattering probability and scattering anisotropy. In Sec. III the spectroscopic evidence of the directional scattering is discussed. In Sec. IV the scattering probability and the scattering anisotropy parameter are extracted from angle-resolved scattering spectra by using the classical approach to light propagation in random inhomogeneous medium. In Sec. V the empirical measure of the scattering anisotropy is introduced and the spectra of the scattering anisotropy are obtained in the vicinity to the first PBG.

II. EXPERIMENTAL TECHNIQUE

Opal films were prepared from a water suspension of polymethylmethacrylate spheres with nominal diameter $D = 398$ nm by crystallizing them in a vertically moving meniscus on a hydrophilic glass substrate followed by opal sintering at $T = 90$ °C.[14]

Angle-resolved transmission spectra were measured at incidence angles θ from 0° to 80° in the standard configuration, where the angle of the incidence is equal to the angle of transmission, with a 2° angular resolution. The samples were illuminated through the glass substrate by a collimated 1 mm in diameter probe beam of white light. Transmission spectra were recorded by using unpolarized light. Samples were mounted taking into account the lattice orientation that was identified by using the surface light diffraction pattern of the opal film.[15] Opal films were oriented so that the increase in incidence angle θ corresponds to scanning the wavevector along the LKL' line on the surface of the opal Brillouin zone.

The scattering was studied using illumination by the same incident beam propagating along the film normal, $\theta = 0°$, which is called below the entry (E) direction. Spectra of the FS light were measured at different angles α from 5° to 75° with respect to the film normal, which are called the exit (X) directions, with a 5° angular resolution behind the opal film and spectra of BS light—from 15° to 75° in front of the film (Fig. 1).

Angle diagrams of the scattered light intensity for any particular wavelength were obtained from angle-resolved spectra of FS and BS light, because in this configuration the size and the brightness of the illuminated sport are maintained constant. Experimental data concerning the scattered light are discussed in comparison to conventional transmission spectra to emphasize the diffraction nature of observed spectral features.

III. SPECTRA OF TRANSMITTED AND SCATTERED LIGHT

Transmission spectra provide the natural basis for comparing the PBG effect upon the scattered light propagating in PhCs. The overview of transmission spectra of the opal film covering two long wavelength PBGs is given in Fig. 2(a). Two branches of minima correspond to the diffraction resonances at crystal planes denoted as 01 and 02 branches.
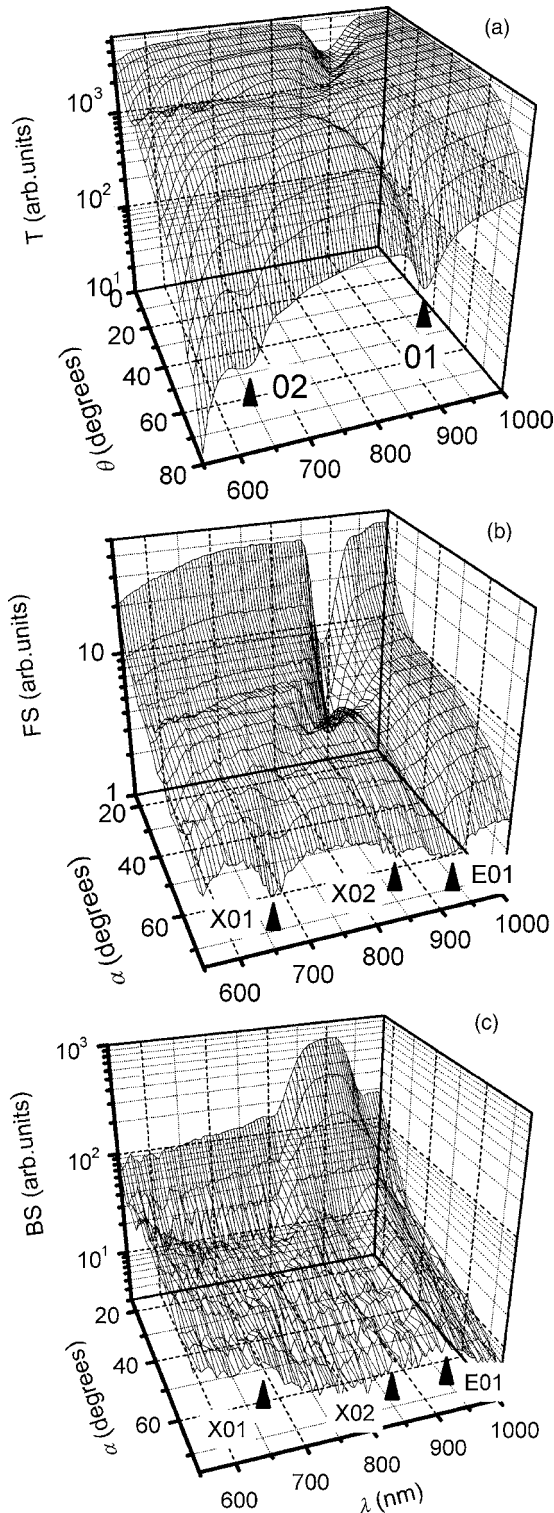
FIG. 2. (a) Transmission spectra of the opal film in unpolarized light showing 01 and 02 PBGs. (b) Spectra of the FS light. (c) Spectra of the BS light. *E*01, *X*01, and *X*02 indicate the diffraction bands along the entry and exit directions.

These branches avoid the crossing at θ angles from 40° to 50°. The transmission magnitude outside the diffraction minima is nearly constant at low incidence angles and decreases toward higher angles and shorter wavelengths. The film thickness $t \approx 7.8$ μm (about 24 bead layers) was estimated from the Fabry–Perot oscillations. This thickness is below the mean free path of photons in opals[1] that gives a

chance for ballistic propagation of photons. At resonance wavelengths, the Bragg attenuation length L_B becomes the characteristic length for the light propagating in PhC. The expression $\Delta\lambda/\lambda_0 = 2 \times 0.816D/\pi L_B$ links the bandgap width $\Delta\lambda$, the central band wavelength λ_0, and the L_B length. Assuming that the relative gap bandwidth is $\Delta\lambda/\lambda_0 \approx 0.056$ (neglecting the term $\Delta\lambda/4\lambda_0$) as calculated for the infinitely large fcc crystal of spheres with the refractive index $n_{sph} = 1.45$ in air,[16] the $L_B = 3.72$ μm applies.

By taking into account the exponential relation between the transmission attenuation ΔI and the film thickness[17] $t = -\ln(1 - \Delta I/I_0)L_B$, where I_0 is the projected intensity in the center of the minimum in the absence of the attenuation, the attenuation in the minimum of the ~ 7.8 μm thick opal film would be as high as eight times in contrast to the experimental value of 2 observed for the 01 minimum. This difference shows a sizable scattered flux mixed with the light transported by opal eigenmodes.[18]

The FS spectra [Fig. 2(b)] obtained in the angle range from 15° to 75° dramatically differ from transmission spectra. First, they show the nondispersive E01 branch of minima. Second, the X01 dispersive branch of minima splits off the nondispersive one at $\alpha \geq 30°$, which also splits at $\alpha \geq 55°$ in two dispersive branches, X01 and X02. The scattered light intensity rapidly decreases with the angle increase, but remains practically independent upon the wavelength along any particular direction. The BS spectra collected in the same range of angles show features, which are, generally, opposite to those in FS spectra [Fig. 2(c)]: There is a broad scattering maximum at low scattering angles, which splits along the angle increase into E01 nondispersive and X01 dispersive branches. At higher angles, the X01 dispersive branch splits again into two X01 and X02 dispersive branches. The BS intensity outside the scattering maxima decreases with increasing angle and gradually increases to shorter wavelengths. It is worthy to note that X02 band is much weaker compared to other bands in FS and BS spectra and can be seen only in the narrow angle range.

To understand the influence of diffraction upon the scattered light propagation, the diffraction features in FS and BS spectra are compared to those in transmission (Fig. 3). The relative attenuation in the 01 transmission minimum at $\theta = 0°$ is $\Delta I/I_0 = 0.52$. The relative light attenuation in the E01 FS minimum at $\alpha = 15°$ is 0.77. The relative height of the E01 BS band is 0.78, i.e., the same as this parameter in the FS spectrum.

The FS and BS spectra are not complementary, since the BS peak is broader than the FS minimum. At $\alpha = 15°$ the relative bandwidth of the E01 FS minimum is $\Delta\lambda/\lambda_0 = 0.059$ against 0.106 bandwidth of the E01 BS band and 0.075 bandwidth of the 01 transmission minimum. In fact, the BS band is the complex one, which consists of two Gaussian lines centered at 863 and 911 nm. These wavelengths correspond, respectively, to the reflectance band at $\theta = 15°$ and the long wavelength edge of the E minimum in the FS and transmission spectra.

At $\alpha = 55°$ the E01 FS minimum remains in the same spectral position, whereas only the long wavelength fraction of the E01 BS band survives. The X01 FS minimum, cen-
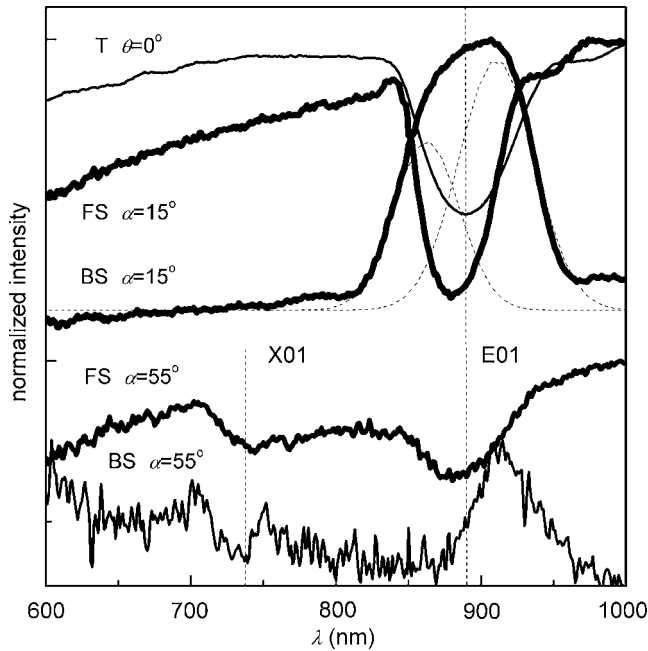
FIG. 3. FS and BS spectra (thick lines) at $\alpha=15°$ and $55°$ in comparison to the transmission spectrum (thin line) along the light incidence direction. Dashed lines show the decomposition of the BS spectrum on Gaussian lines.

tered at 737 nm, is repeated in the BS spectrum, as a minimum surrounded by two weak peaks (Fig. 3). Further development of this tendency expels the maximum of the $X01$ BS band to the short wavelength edge of the $X01$ FS minimum.

Dispersion of transmission minima was analyzed against the Bragg law $\lambda_{hkl}=2d_{hkl}n_{\mathrm{eff}}\sqrt{1-\sin^2 r_{hkl}}$ in association with the Snell law $n_{\mathrm{eff}} \sin(r_{111})=n_{\mathrm{air}} \sin(\theta)$, where r_{111} and θ are the internal and external angles of light propagation, d_{hkl} is the interplane distance along the $[hkl]$ direction, and n_{eff} is the effective refractive index. Approximation of the 01 branch of transmission minima by diffraction at (111) planes (Fig. 4) gives the sphere diameter $D=403$ nm in correspondence to microscopy data and $n_{\mathrm{eff}}=1.351$. The diffraction
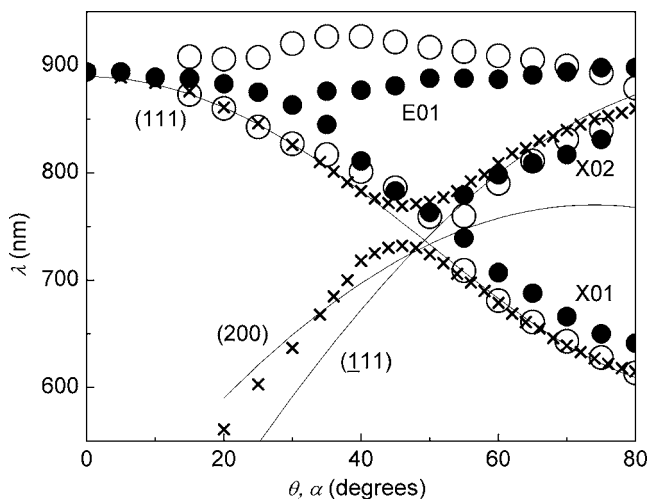

FIG. 4. Dispersions of diffraction bands in FS (solid circles) and BS spectra (empty circles) in comparison to dispersions of diffraction minima in transmission spectra (crosses). Lines show the Bragg law fits to transmission minima dispersions.

model provides a realistic description of the transmission minima dispersion except the angle range from 42° to 52°, where the multiple wave diffraction takes place.[19] Projected dispersions of diffraction resonances at ($\bar{1}11$) and (200) planes were obtained by using the estimated opal parameters. Neither of them precisely fits the 02 branch of minima. In the context of the present investigation, this observation can be associated with large-scale lattice defects, like $...ABCCBA...$ stacking faults along the [111] axis of the fcc lattice, leading to averaging of ($\bar{1}11$) and (200) diffraction resonances in the spectra.

The $E01$ nondispersive branches of FS and BS bands correspond to the diffraction minimum at $\theta=0°$. The $E01$ BS bands slightly deviate from this position by developing up to 30 nm redshift. The $X01$ dispersive branches precisely follow the (111) diffraction resonance and $X02$ branches—the 02 resonance. The $X01$ FS minima are "redshifted" by, approximately, 35 nm from the (111) diffraction minima (Fig. 4).

Correlation between bands in the spectra of scattered and transmitted light suggests that bands in scattering spectra originate from diffraction of the scattered light in the opal crystal.[9,12] By taking into account the geometry of the experiment, the E branch can be associated with the diffraction of the incident beam, whereas the X branch—to the diffraction of the scattered light along the detection direction.[20] In contrast to the dispersion of minima in transmission, the dispersion of minima in the FS follows the Bragg law without noticing the multiple wave diffraction. This observation supports the assumption that scattered light is transported by defect modes.

Simultaneous observation of the E and X diffraction features in scattering spectra suggests that the scattered light trajectory is, effectively, a composition of two parts with wavevectors of the incident and the detected beams. This path memory effect is equivalent to the scattering order $N=1$.

The analogy between transmission and FS spectra is straightforward, since FS spectra accumulate all diffractive bands along the E and X directions. In contrast, the analogy between BS and reflectance spectra is invalid, since the reflectance spectra detect only those diffraction bands, which appear along the direction of the mirror reflectance, whereas the BS spectra accumulate the diffraction orders likewise the transmission spectra. Another striking observation is the exceptionally high magnitude of the BS light intensity, which should be much weaker than the FS intensity in the case of the low-order scattering.

These observations allow us to reconstruct the scattering process. Figure 5 illustrates two models. The common features of these models are the backdiffracted E-band in reflectance and E- and X-minima in transmission. Moreover, the $E01$ bands in reflectance and transmission are equivalent. Model 1 assumes that scattering event, denoted as collision 1, occurs in the opal film. Then, the FS spectrum resembles a linear superposition of transmission spectra along the beam incidence and detection directions. In the BS spectrum three bands overlay: (i) the minimum due to backdiffracted $E01$
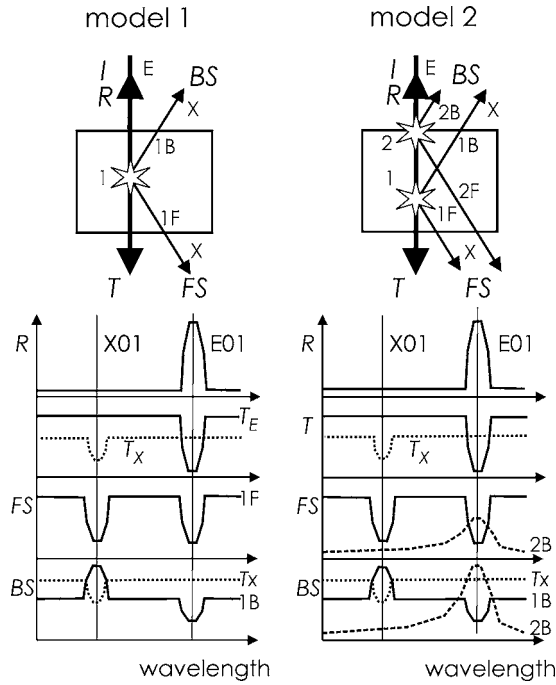
model 1   model 2

FIG. 5. Formation of scattering spectra. Model 1 considers only scatterers (collision 1) inside the PhC film. Model 2 considers combined effect from internal (collision 1) and surface (collision 2) scattering. 2B, 1B, and 1F denote the trajectories of the detected photons in the forward (F) and backward (B) directions from corresponding sources (collision 1 or 2). E and X are entry and exit directions.

band, (ii) the $X01$ maximum due to zero order diffraction in reflectance applied to the 1XF light path, and (iii) the $X01$ transmission minimum applied to the 1XB path. $X01$ bands in transmission and reflectance cancel each other, that explains their weak appearance in the experimental BS spectrum.

However, model 1 fails to reproduce the overall high intensity of the BS light, in general, and strong $E01$ band in BS spectra, in particular. This circumstance leads us to add the more isotropic scattering, compared to the highly directional E-band, at the surface of a PhC film, denoted as collision 2 in model 2. The surface scattering of a collimated incident beam explains the isotropy of the E-band in BS spectra and smearing the E-band in the high angle FS spectra. The main component of this band is the uncoupled light, which originates from mismatch of PhC eigenmodes and a mode continuum of free space. This source of scattered light appears due to specific properties of PhCs and it does not apply to random inhomogeneous media. The intensity of uncoupled light peaks around the PBG along the direction of the incident beam, which is the [111] axis in the fcc lattice of the opal crystal. Nevertheless, this band spreads toward shorter wavelengths due to contribution from uncoupled scattered light (Fig. 5). The intensity of uncoupled scattered light rapidly reduces with the angle increase. This mechanism explains the 863 nm subband in the BS spectrum at α =15° (Fig. 3). It may also response to the mobility edges spreading over the PBG edges in disordered PhCs.[21]

The $X02$ band in BS spectra can be treated similar to the appearance of the multiple Bragg diffraction in reflectance, taking into account that the angle width of a cone of scat-
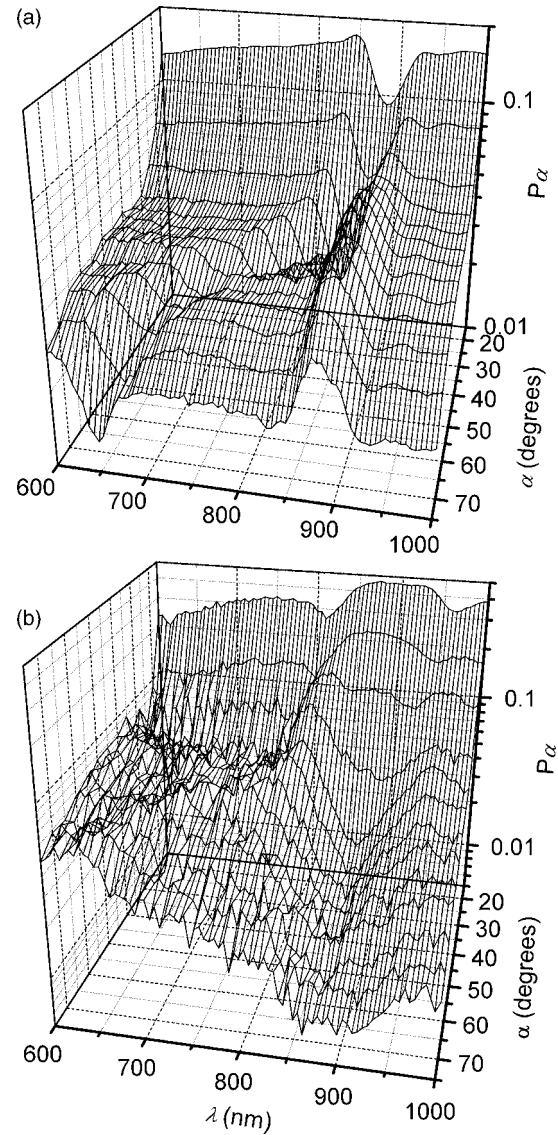

FIG. 6. Spectra of FS (a) and BS (b) scattering probabilities.

tered light is broader than that of the diffraction one and the 6° wide range of internal angles of light propagation, in which the $X02$ band is observed.

The spectral shift of similar bands in FS and BS spectra may relate to the details of the light propagation, for example, the difference in refraction for type 1 and 2 sources of scattered light, and the different angle dependence of the aperture of collecting optics.

IV. SCATTERING PROBABILITY AND ANISOTROPY

The spectra of the probability P_α of light scattered to a given angle were obtained by dividing the spectrum measured at a given angle to the sum of such spectra for all angles (Fig. 6). This is a simplification, which assumes the axial isotropy of scattered light spectra with respect to the [111] axis. The angle range 0°–10° along the film normal was excluded from the analysis to avoid taking transmitted/ reflected beams of high intensity into consideration. It should be noted that the resulting probability spectra qualitatively remain the same for the total scattered light intensity accu-
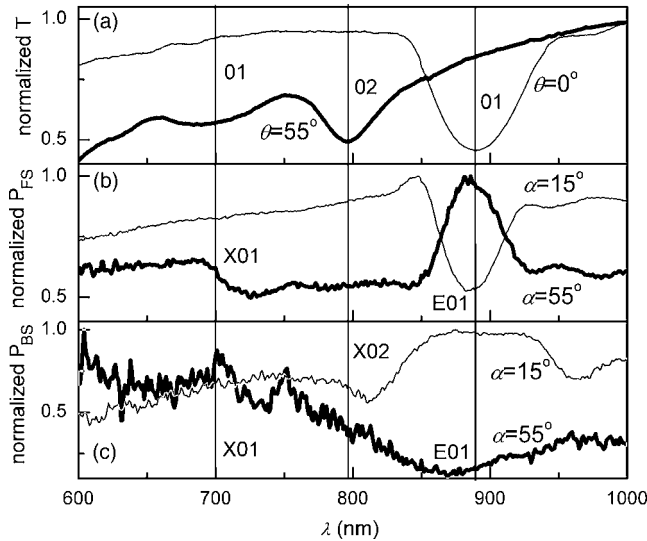
FIG. 7. Normalized transmission spectra for the normal and oblique light incidence (a) and spectra of normalized forward (b) and backward (c) scattering probability at different angles of the light detection. Angles are shown at the curves. Vertical lines highlight correlations of E01 and X01, X02 features in the scattering spectra with 01 and 02 diffraction minima in transmission spectra.

FIG. 8. Spectra of the FS and BS anisotropies obtained from classical scattering model.

mulated for angle ranges 5°–80°, 10°–80°, and 15°–80°. This argument suggests that calculated probability spectra are stable and demonstrate the essential properties of the light propagation in opal films. However, the magnitude of the scattering probability in this approximation is the relative value, which depends on the choice of total scattered intensity. Similar procedures were applied to FS and BS spectra to allow the comparison.

By definition, the probability spectra compare the scattering intensity along the particular direction and the total scattering intensity at the same wavelength. Correspondingly, diffraction bands in probability spectra express the relative strength of the diffraction attenuation of the light scattered to a given angle compared to the diffraction fingerprint in the angle-integrated spectrum. At low scattering angles $\alpha < 25°$ the diffraction suppresses the FS probability, but at $\alpha > 35°$ probability spectra contain one minimum and one maximum [Figs. 6(a) and 7(b)] centered at the same wavelengths as corresponding minima in FS spectra. The higher than the off-resonance P_α value is assigned to $E01$ scattering band at $\alpha > 25°$, provisionally, due to the stronger contribution of diffuse scattered light in the high angle FS spectra. The lower P_α is associated with the dispersive $X01$ band due to the absence of this feature in the integrated scattering spectrum.

In reverse to the FS probability, the broad maximum is seen in BS P_α spectra at $\alpha < 25°$ [Figs. 6(b) and 7(c)]. At higher angles, this maximum splits in the minimum for the $E01$ branch and the maximum for the dispersive $X01$ branch. As opposite to the FS anisotropy, the probability of BS scattering at diffraction bands along the X direction is higher than the off-resonance scattering probability and along the E direction—is lower [Fig. 7(c)]. The interpretation of these features remains the same as in the case of the forward scattering.

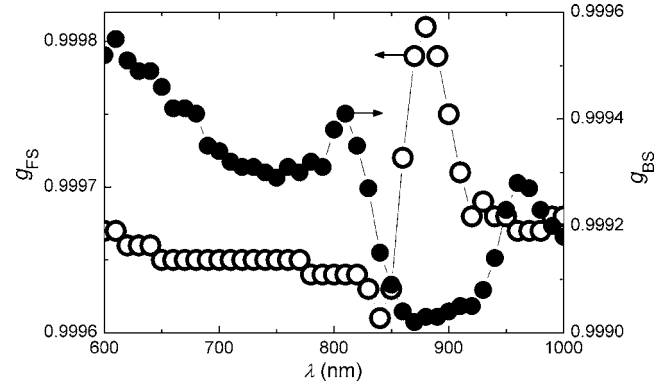Scattering anisotropy expressed by $p(\cos \alpha)$ function

was obtained from scattering probability by using expression (3). Then, the anisotropy parameter of scattering, g, was calculated from $p(\cos \alpha)$ by using Henyey–Greenstein function (2) (Fig. 8). Overall $g \leq 1$ value applies to both FS and BS spectra. The high value of the anisotropy parameter points to the directional character of light scattering in thin opal films. This conclusion assumes that large size defects dominate the light scattering in thin opal films.

In the case of the FS light, the g-spectrum shows a narrow peak in the PBG range for the light incidence direction and a small minimum at the short wavelength edge of this peak. In the case of BS light, the g-spectrum shows a broad minimum in the same range and two peaks at the edges of this minimum. Generally, the BS g-spectrum is opposite to that in the FS light and demonstrates the much broader band. It is instructive to emphasize the fact that in accord to the classical scattering model, the higher FS probability is accompanied by the lower BS probability and vice versa.

The g-spectra (Fig. 8) assign the highest FS and the lowest BS directionality to the PBG spectral range. This observation agrees the scattering probability at low scattering angles, but contradicts the scattering probability at high scattering angles (Fig. 6). To investigate and resolve this issue the examination of the scattering indicatrix is necessary.

V. DIAGRAMS OF THE SCATTERED LIGHT PROBABILITY AND INTENSITY

In Fig. 9 the $p(\cos \alpha)$ functions are shown against the scattering angle α for the wavelengths inside and outside the PBG range along the light incidence direction. The modulation superimposed on experimental diagrams corresponds to the diffraction bands in FS and BS light.[9] Curve 1 is the Henyey–Greenstein fit [expression (2)], which allows to extract the anisotropy parameter g as the fitting parameter. In all diagrams of FS and BS light, the Henyey–Greenstein fit is captured by scattering anisotropy/probability at low angles. Deviation of this fit from experimental points at angles $\alpha > 30°$ indicates the essential contribution of high orders of scattered light.

Curve 2 is the hyperbolic fit $p \sim p_0 \alpha^{-k_P}$, where p_0 is the anisotropy of the light scattering at $\alpha = 15°$ and k_p is the
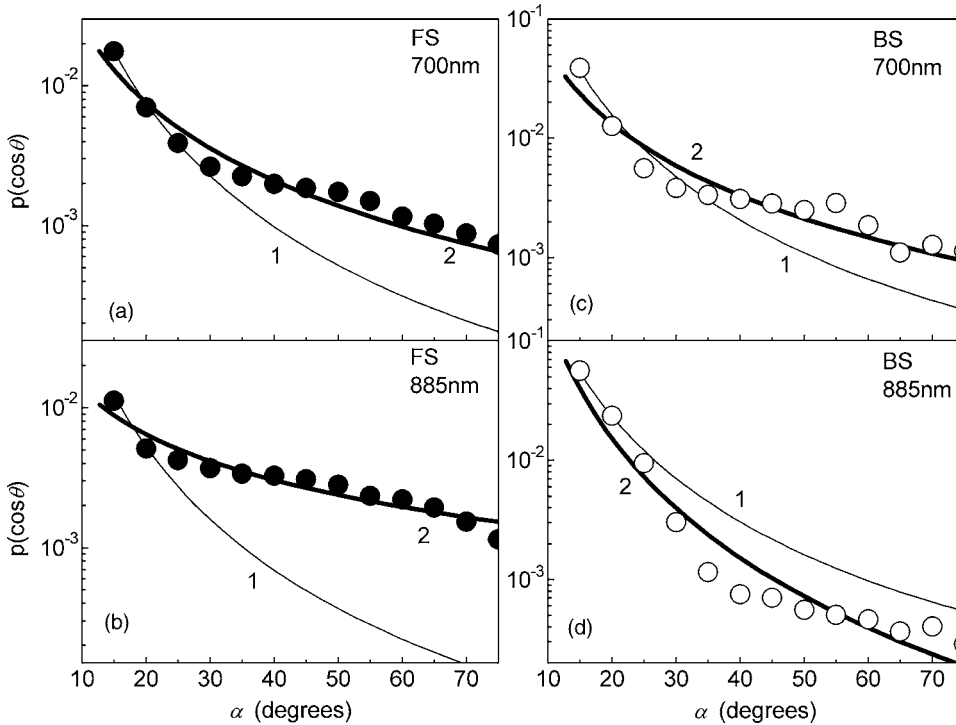
FIG. 9. Scattering anisotropy diagrams at $\lambda=700$ and 885 nm and their approximations by the Henyey–Greenstein function (curve 1) and by the hyperbolic fit (curve 2) for FS [(a) and (b)] and BS [(c) and (d)] light.

exponent. Obviously, the hyperbolic fit approximates experimental $p(\cos \alpha)$ data more accurately in a wide range of scattering angles (Fig. 9).

Both g and k_p spectra for the FS light demonstrate a strong peak in the PBG range, but the essential difference is the opposite signs of g and k_p values, i.e., they describe opposite tendencies [Fig. 10(a)]. It is worthy to also emphasize the dramatic difference in the resolution of the peak—the relative height of this peak in the g-spectrum is 1.6 $\times 10^{-4}$ against 0.31 in the k_p spectrum. In the BS anisotropy spectra the relationship between g and k_p spectra is the same as for the FS light: coincidence of the main bands taken with opposite signs and washing out spectral features at PBG edges in the k_p spectrum [Fig. 10(b)].

Further insight in the analysis of the scattered light directionality can be achieved, if the hyperbolic description $I \sim I_0 \alpha^{-k_I}$ is applied to the angle diagrams of the scattered light intensity [Figs. 2(b) and 2(c)]. The corresponding spectrum of the k_I exponent follows in detail the spectrum of the k_p exponent (Fig. 10). Moreover, the diffraction resonance resolution increases further in the k_I-spectrum to 0.62. In the BS light the diffraction resonance resolution improves from 3×10^{-4} to 0.26 and to 0.38 in g, k_p, and k_I spectra, respectively, in agreement with the tendency observed for the FS light.

The k_I-spectrum has a straightforward physical explanation—the k_I value is a measure of the angle width of the scattering indicatrix. As a result, the lower the scattering anisotropy, the broader the indicatrix and the lower the $|k_I|$ absolute value. This is an empiric way to measure the scattering strength. Owing to the opposite sign of the k-exponent, as compared to the g-factor sign, the inconsistency between the scattering anisotropy and scattering probability revealed in the previous section can be resolved. Namely, the broadening of the FS diagram, i.e., lower anisotropy of scattering,
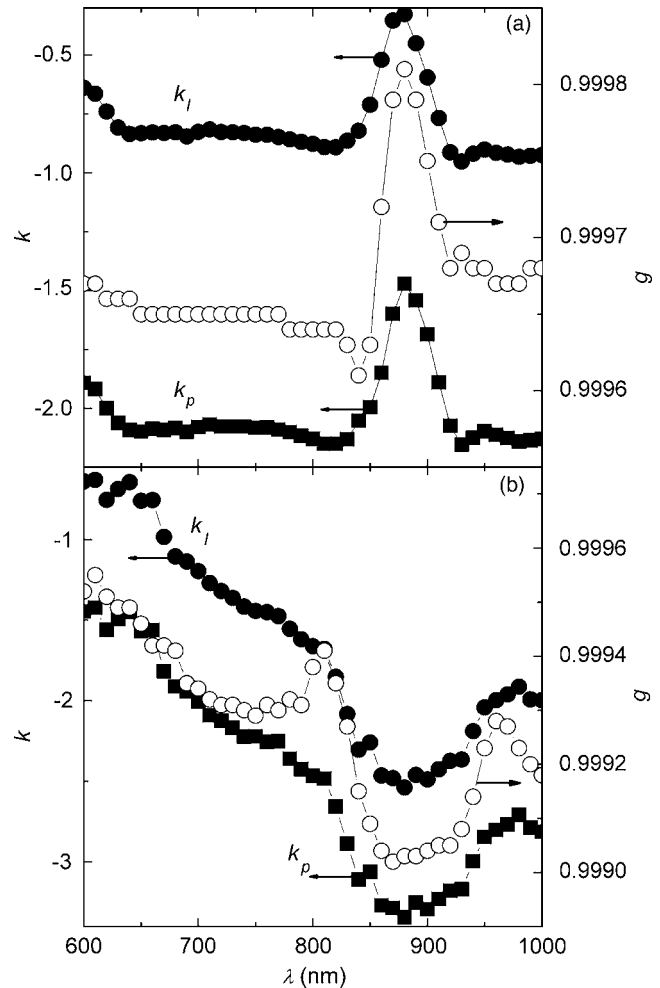

FIG. 10. Spectra of g parameter (empty circles) in comparison to spectra of exponents k_P and k_I for FS (a) and BS (b) light.

occurs at the diffraction resonance for the incident light and corresponds to the lower transparency of the opal film. The physical reason for this effect is, provisionally, the substitution of the l_{tr} length with much shorter L_B length in the relevant spectral and angle ranges that leads to more efficient scattering.

Oppositely, the stronger BS anisotropy takes place at the diffraction resonance because of the intense generation of uncoupled light in the PBG vicinity. To the short wavelength end of the measured spectra, the BS indicatrix becomes much broader following the opaque appearance of the opal in this spectral range. The k_I bandwidth is $\Delta\lambda/\lambda_0 = 0.04$ in the FS light and is 0.12 in the BS light. Here we see the correspondence between the backward diffraction of the surface scattered light (Fig. 3) and the scattering anisotropy (Fig. 10).

Thus, the k_I-spectrum is the generalized representation of the opal transparency in the forward direction or its opalescence in the backward direction. Compared to g-factor, which takes into account low-order scattering, the k_I-exponent approximates the scattering of different orders. This circumstance makes exponent more sensitive to the details of light scattering leading to the stronger spectral variation of k_I-values with changes of the regime of the light propagation.

VI. SUMMARY

Combined analysis of angle-resolved spectra of the forward and backward scattered light in thin opal-based PhCs allowed uncovering specific light scattering phenomena in PhCs with predominately ballistic regime of light propagation. It was shown that the model of scattering in random inhomogeneous medium correctly identifies the high anisotropy of scattering in such PhCs. However, this model fails to explain the observed spectra of scattering anisotropy, to quantify this anisotropy, and to estimate the magnitude of backscattered light because it is not adopted to describe the scattering in well-ordered lattices with low defect density, in which the scattering mechanism changes with the wavelength, the scattering order depends on the direction, and the eigenmodes are different from mode continuum of free space.

As the first approximation, the simple model of light scattering in thin PhCs was proposed, which includes the low scattering order process leading to light path memory and strong scattering anisotropy and the additional source of scattered light due to uncoupled light at a PBG spectral range. In order to quantify the scattering anisotropy the use of the exponent of the hyperbolic fit to scattered light indicatrix was suggested. More adequate description of scattering phenomena observed in the regime $t < l_{tr}$ requires numerical modeling of light propagation in 3D PhCs with variable defect size and density.

[1] A. F. Koenderink, A. Lagendijk, and W. L. Vos, Phys. Rev. B **72**, 153102 (2005).
[2] A. Isimaru, *Wave Propagation and Scattering in Random Media* (Academic, New York, 1978), Vols. 1 and 2.
[3] L. Henyey and J. Greenstein, Astrophys. J. **93**, 70 (1941).
[4] S. E. Skipetrov and S. S. Tchesnokov, Quantum Electron. **25**, 753 (1998).
[5] M. Y. Kirillin and A. V. Priezih, Quantum Electron. **32**, 883 (2002).
[6] Y. Xia, B. Gates, Y. Yin, and Y. Lu, Adv. Mater. (Weinheim, Ger.) **12**, 693 (2000).
[7] M. A. Kaliteevski, J. Manzanares Martinez, D. Cassagne, and J. P. Albert, Phys. Rev. B **66**, 113101 (2002).
[8] V. N. Astratov, A. M. Adawi, S. Fricker, M. S. Skolnick, D. M. Whittaker, and P. N. Pusey, Phys. Rev. B **66**, 165215 (2002).
[9] A. F. Koenderink and W. L. Vos, Phys. Rev. Lett. **91**, 213902 (2003).
[10] J. F. Galisteo-Lopez, E. Palacios-Lidon, E. Castillo-Martinez, and C. Lopez, Phys. Rev. B **68**, 115109 (2003).
[11] S. G. Romanov, JETP Lett. **79**, 614 (2004).
[12] S. G. Romanov and C. M. Sotomayor Torres, Phys. Rev. E **69**, 046611 (2004).
[13] Yu. A. Vlasov, V. N. Astratov, A. V. Baryshev, A. A. Kaplyanskii, O. Z. Karimov, and M. F. Limonov, Phys. Rev. E **61**, 5784 (2000).
[14] P. Jiang, J. F. Bertone, K. S. Hwang, and V. L. Colvin, Chem. Mater. **11**, 2132 (1999).
[15] J. F. Galisteo, F. Garcia-Santamaria, D. Golmayo, B. H. Juarez, C. Lopez, and E. Palacios, J. Opt. A, Pure Appl. Opt. **7**, S244 (2005).
[16] A. Reynolds, F. Lopez-Tejeira, and D. Cassagne, Phys. Rev. B **60**, 11422 (1999).
[17] J. F. Bertone, P. Jiang, K. S. Hwang, D. M. Mittleman, and V. L. Colvin, Phys. Rev. Lett. **83**, 300 (1999).
[18] J. F. Galisteo Lopez and W. L. Vos, Phys. Rev. E **66**, 036616 (2002).
[19] S. G. Romanov, T. Maka, C. M. Sotomayor Torres, M. Müller, R. Zentel, D. Cassagne, J. Manzanares-Martinez, and C. Jouanin, Phys. Rev. E **63**, 056603 (2001).
[20] S. G. Romanov, C. M. Sotomayor Torres, M. Egen, and R. Zentel, Photonics Nanostruct. Fundam. Appl. **4**, 59 (2006).
[21] S. John, in *Photonic Band Gap Materials*, edited by C. M. Soukoulis (Kluwer, Dordrecht, 1995), p. 563.